· Article · Advances in Polar Science
doi: 10.12429/j.advps.2022.0016 September 2023 Vol. 34 No. 3: 165-176

Analysis of the record-breaking August 2021 rainfall over the Greenland Ice Sheet

DOU Tingfeng[1*], XIE Zuowei[2], Jason E. BOX[3*], YANG Qing[2], YANG Yifan[1], TENG Shiwen[4], XU Gaojie[1], LIU Chao[4], LI Xichen[2], Derek HOUTZ[5], GONG Xun[6], DU Zhiheng[7], DING Minghu[8], YU Yongqiang[2] & XIAO Cunde[9*]

[1] College of Resources and Environment, University of Chinese Academy of Sciences, Beijing 100049, China;
[2] Institute of Atmospheric Physics, Chinese Academy of Sciences, Beijing 100029, China;
[3] Geological Survey of Denmark and Greenland (GEUS), Copenhagen 1350, Denmark;
[4] Key Laboratory for Aerosol-Cloud-Precipitation of China Meteorological Administration, School of Atmospheric Physics, Nanjing University of Information Science & Technology, Nanjing 210044, China;
[5] Swiss Federal Institute for Forest, Snow and Landscape Research (WSL), Birmensdorf CH-8903, Switzerland;
[6] Hubei Key Laboratory of Marine Geological Resources, China University of Geosciences, Wuhan 430074, China;
[7] State Key Laboratory of Cryospheric Science, Northwest Institute of Eco-Environment and Resources, Chinese Academy of Sciences, Lanzhou 730000, China;
[8] Institute of Global Change and Polar Meteorology, Chinese Academy of Meteorological Sciences, Beijing 100081, China;
[9] State Key Laboratory of Earth Surface Processes and Resource Ecology, Beijing Normal University, Beijing 100875, China

Received 22 August 2022; accepted 4 December 2022; published online 30 June 2023

Abstract Rainfall was witnessed for the first time at the highest area of the Greenland Ice Sheet on 14 August, 2021. The thermodynamic mechanisms supporting the rainfall are revealed by ERA5 reanalysis, in-situ and satellite data. We find that a strong southward intrusion of the polar vortex favored the maintenance of a deep cyclone over Baffin Island and an amplification of anticyclonic circulation over the southeastern ice sheet, which pumped warm and moist air toward Greenland from anomalously warm waters south of Greenland. Across a wide swath of the ice sheet, atmospheric uplift maintained above-melting and rainfall conditions via condensation and enhanced downward infrared irradiance. Without the low-level liquid clouds, the spatial extent and duration of the rainfall would have been smaller. Over the ice sheet topographic summit, the air temperature from the ground to 250 hPa level was ~2 °C higher than the previous record set on 12 July, 2012. Such events may occur more frequently with the decreased temperature contrast between the Arctic and the mid-latitude regions that drives highly amplified jet streams. Thus, this extreme event serves as a harbinger of a more likely wet surface condition across all elevations of the ice sheet.

Keywords **Greenland Ice Sheet, rainfall, polar vortex, liquid cloud**

Citation: Dou T F, Xie Z W, Box J E, et al. Analysis of the record-breaking August 2021 rainfall over the Greenland Ice Sheet. Adv Polar Sci, 2023, 34(3): 165-176, doi: 10.12429/j.advps.2022.0016

1 Introduction

On 14 August, 2021, an anomalously high Greenland Ice Sheet melt extent of 872000 km^2 (Scambos et al., 2021) had rainfall witnessed for the first time at Summit Station (72.58°N, 38.46°W, 3216 m above sea level) near the highest point of the ice sheet, arousing international attention (Ramirez, 2021).

Rainfall events are common over the lower reaches of the ice sheet in summer and into September (Niwano et al.,

* Corresponding authors, ORCID: 0000-0003-0664-8732, E-mail: doutf@ucas.ac.cn (Dou T F); jeb@geus.dk (Box J E); ORCID: 0000-0002-1706-4794, cdxiao@bnu.edu.cn (Xiao C D)

2021). Not only do they contribute to surface ablation processes by reducing the albedo and increasing the density and temperature of near-surface snow and ice (Reijmer et al., 2012; Rennermalm et al., 2013; Vandecrux et al., 2020; Box et al., 2022), they can impact ice flow dynamics and meltwater runoff (Doyle et al., 2015). Rainfall has been increasing across the Arctic under global warming (Han et al., 2018; Dou et al., 2019, 2021, 2022; McCrystall et al., 2021). It is reasonable to consider that rainfall far inland on the ice sheet is extremely unlikely due to its extreme high altitude, average low precipitable water vapor, long distance from the oceans and the extremely low inland surface temperatures. This study investigates the causes for this rainfall event over the highest area of Greenland by considering the large-scale atmospheric circulation driving the warm and moist air (WMA), and the cloud physical processes over the ice sheet.

2 Data and methods

2.1 Automatic weather station observations

2.1.1 Air temperature and albedo observed at Summit Station

The Summit Station (Figure 1a), an automatic weather station (AWS) of the Greenland Climate Network (GC-Net), has monitored surface micro climatological and glaciological parameters since the mid-1990s (Steffen et al., 1996). The AWS is equipped with a temperature sensor with an accuracy of better than 0.3 °C and a sampling interval of 15 s. The albedo was calculated based on the observations from LI-200SZ pyranometers using a running ± eleven-hour sum of upward/downward solar irradiance after van den Broeke et al. (2004). Hourly-averaged 2 m air temperatures during 1995–2021 were used to obtain the frequency and the corresponding date of the near-surface temperature reaching the melting point since 1995. Hourly-averaged albedos during 11–18 August, 2021 were used to verify the occurrence of rainfall.

2.1.2 Rainfall amount observed at Crawford Point AWS

Here, we exploit the rainfall observations from the Lufft WS401-UMB sensor package that the Geological Survey of Denmark and Greenland (GEUS) has included in a new generation of GC-Net AWS since June, 2021 at e.g., Crawford Point 1 (CP1, 69.52°N, 47.02°W, 1941 m, Figure 1a). Precipitation gauge undercatch errors are corrected after Yang et al. (1999).

2.2 Cloud physical characteristics observed by satellite

The data of cloud physical characteristics are obtained from NOAA (National Oceanic and Atmospheric Administration) Climate Data Record (CDR) of AVHRR (Advanced Very High Resolution Radiometer) reflectance and brightness temperatures, which was produced by the University of Wisconsin using the AVHRR Pathfinder Atmospheres–Extended (PATMOS-X) Version 5.3 processing system (Pinzon and Tucker, 2014; Key et al., 2015). Since 1979, NOAA and MetOp satellite have passed between twice and 10 times every day, covering the entire globe. This study uses the data of cloud type, cloud temperature and cloud top height from the MetOp platform on 13 and 14 August (Indexof/data/avhrr-reflectance-cloud-properties-patmos-extended/access(noaa.gov)). Note that the observed supercooled water cloud refers to liquid cloud droplets below 273.16 K (Pavolonis et al., 2005). The source (raw, Level 2) AVHRR data points, with a sensor resolution of 1.1 km near nadir, have been gridded to a 0.1°×0.1° equal-angle grid in ascending and descending files. These data include calibrated reflectance channels in the visible spectrum (0.63, 0.86, and 1.6 microns) portion of the record, brightness temperatures from the 3.75, 11 and 12 μm channels as well as a suite of cloud products (the PATMOS-x Cloud Properties CDR).

2.3 ERA5 reanalysis data of circulation, water vapor flux, air temperature and cloud

ERA5 is the fifth generation ECMWF reanalysis of the global climate and weather (Hersbach et al., 2020) (https://cds.climate.copernicus.eu/cdsapp#!/search?type=dataset), which is produced at a 1-hourly time step using an advanced 4D-Var assimilation scheme with a horizontal resolution of approximately 31 km, including variables on 37 pressure levels from 1000 hPa to 1 hPa. Here used are geopotential height, winds, specific humidity air temperature and potential vorticity (https://cds.climate.copernicus.eu/cdsapp#!/dataset/reanalysis-era5-pressure-levels? tab=overview), and the following variables on single levels: total precipitation, snowfall, sea level pressure and 10 m horizontal wind (https://cds.climate.copernicus.eu/cdsapp#!/dataset/reanalysis-era5-single-levels?tab=form). The temperature data of the middle 26 layers (700 hPa to 100 hPa) were used to analyze the daily vertical profile of air temperature at Summit Station on the warmest day per year since at least 1995.

For cloud investigations, the ECMWF Integrated Forecasting System (IFS) cloud scheme simplifies water droplets of different sizes to represent a number of discrete cloud droplets/particles, including cloud water droplets and raindrops. The 'Total column cloud liquid water' variable represents the amount of liquid water contained within cloud droplets in a column from the ground to the top of the atmosphere, and it is used to reproduce the development of liquid-phase cloud over Greenland. The specific cloud liquid water content and geopotential are applied to determine the height of liquid-phase cloud. Hourly ERA5 cloud data during 13–15 August, 2021 are used.

2.4 Methods

We adopt the Lagrangian analysis tool LAGRANTO

developed by Sprenger and Wernli (2015) to calculate the 4-day backward trajectories for the rainfall event. LAGRANTO was driven by 2-hourly wind fields on a (0.25°×0.25°) grid and 27 pressure levels. Trajectories were started from 1400 UTC (the warmest time) on 14 August, 2021 at 50 hPa above the ground level. The starting grid points had a 10 km spacing, sampled with radius 50 km around the summit of Greenland (38.46°E, 72.58°N). The end grid point was the corresponding starting grid point four days before.

The following methods were used in the calculation of water vapor convergence over the ice sheet. Moisture flux ($\vec{Q} = q\vec{V}/g$) was equal to the horizontal wind ($\vec{V}$) multiplied by the specific humidity (q) on pressure levels and then divided by the gravitational constant (g). It was used to represent the source, direction and intensity of water vapor transport. Moisture flux divergence ($\nabla \cdot \vec{Q}$) usually characterizes the degree of water vapor concentration change caused by atmospheric movement. Positive and negative values indicate divergence and convergence of water vapor, respectively. Vertically integrated moisture flux divergence from surface to the cloud top ($\nabla \cdot \frac{1}{g}\int_{P_{\mathrm{sfc}}}^{P_{\mathrm{cloud\_top}}} q\vec{V}\mathrm{d}p$) can clearly reflect the amount of water vapor change in a specific area, thus has a good corresponding relationship with surface precipitation.

3 Results

3.1 Background atmospheric circulation during the precipitation event

Figure 1a illustrates the spatial distribution of Greenland Ice Sheet precipitation on 14 August, 2021 from the ERA5 reanalysis, which coincides with the melt extent of the ice sheet surface observed by the satellite record during the same period (Scambos et al., 2021). The circulation field during this precipitation event had leaded to an abnormally high temperature and water vapor content from a southwesterly WMA intrusion (Figure 1b). The intrusion caused a near-surface warming of 9 °C in average for the area above 1000 m surface elevation relative to the climatology. The vertical profiles of air temperatures demonstrated that the warming caused by the WMA was not only occurring in the planetary boundary layer, but extended throughout the troposphere to 250 hPa with about 2 °C higher temperatures than the highest daily temperature profile on 12 July, 2012 (Figure 1c).

The front edge of the warm air converged with a weak westerly wind, causing the precipitation belt to advance to the inland area (Figure 1b). The rainfall area generally coincided with the areas with sufficient moisture supply simulated by ERA5, and they were larger (more northerly) than the areas with near surface warming to the melting point (Figures 1a, 1b). The precipitation was sustained by topographic uplift of a warm front with non-convective precipitation (Figure S1). Upstream, over the steeper slopes of the southwestern ice sheet, ERA5 indicates that the precipitation included a convective process (Figure S1c), resulting in a relatively heavy local precipitation above 20 mm·d^{-1} (Figure 1a), which was partly verified by the observation of 15 mm at the CP1 Station during the same period.

3.2 The formation and maintenance of anomalous atmospheric circulation

The key atmospheric circulation responsible for the northward advection of WMA was a low pressure system located over the Baffin Island on 14 August, 2021 (Figure S2). To explore its evolution, we investigated the mid-tropospheric daily mean 500 hPa geopotential heights, sea level pressure and the dynamic perspective from 330 K potential vorticity and horizontal wind from 10 to 14 August, 2021 (Figure 2). The potential vorticity advection on an isentropic surface was conserved following the adiabatic and frictionless flow and thus could concisely illustrate the formation and enhancement of a trough or ridge (Figure 2). The 330 K isentropic surface inclined gradually from the Arctic to a lower latitude, along which a circulation veers to be more rotating by moving equatorward.

On 10 August, the polar vortex was displaced toward North America with a low pressure center (SLP: 980 hPa) extending to the surface over the Baffin Island (Figure 2a). Such a strong circulation was effective to deliver WMA toward Greenland, preconditioning the occurrence of rainfall. Meanwhile, a trough was extended from the polar vortex southeastward over North America. Due to the high potential vorticity advection from the north into the trough (Figures 2d, 2e), this trough was subsequently isolated from the polar vortex to a closed low over the Hudson Bay with an intensification of the surface cyclone on 12 August (Figures 2b, 2e). In the eastern flank of this closed low, the southerly flow advected low potential vorticity toward the Baffin Bay and amplified the ridge from Newfoundland to the Baffin Bay (Figure 2e).

As shown in Figures 2c and 2f, the closed low pressure system retreated poleward due to the northward advection of low potential vorticity on 14 August. Meanwhile, a ridge was amplified from the North Atlantic northward to Greenland. As a result, southwesterly flow between the closed low and the ridge prevailed from the mid-troposphere to the surface, which intensively transported WMA to Greenland, leading to much warmer vertical profile than those of previous extreme high temperature events in this region (Figure 1c). Such strong and long-lasting water vapor transport was also known as an atmospheric river (AR) (Newell et al., 1992; Eckhardt et al., 2004; Ralph et al., 2004). Neff et al. (2014) identified

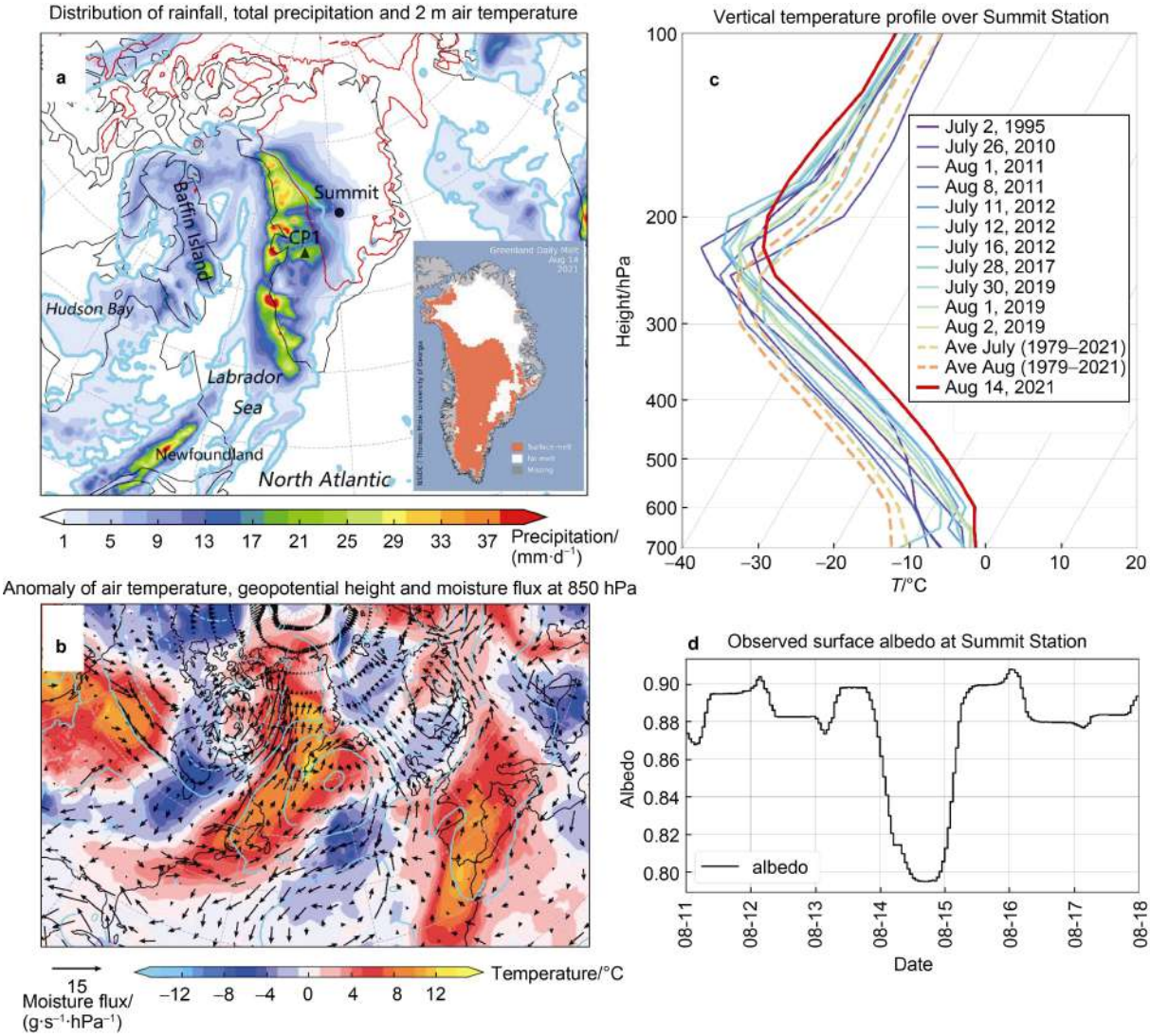

Figure 1 Process analysis of the August 2021 rainfall event. **a**, Distribution of daily mean total precipitation (shaded) and 2 m air temperatures (contour) in the Greenland region on 14 August, 2021 from ERA5 reanalysis. The cyan contours mark the 1 mm·d^{-1} rainfall isoline, and the red contours indicate the 0 °C 2 m air temperature isotherm. The inset map illustrates the melt extent of the ice sheet surface during the rainfall event observed by the SSM/I satellite (Scambos et al., 2021); **b**, Large-scale atmospheric circulation features of the rainfall event, including anomalies of daily mean air temperature (shaded), geopotential height (contour) and moisture flux (arrow) at 850 hPa, relative to the same period of 1979–2020 mean; **c**, The vertical air temperature profile at Summit Station on the warmest day per year since at least 1995 based on ERA5, the thick red line indicates the profile on the day of August 2021; **d**, The hourly variations in surface albedo observed at the Summit GC-Net AWS from 11 to 18 August, 2021.

ARs promoting Greenland melting by advection of air masses over the ocean with upstream development over the 2012 summer North American heatwave. These 2012 ARs were responsible for the largest single-day Greenland-wide surface ice ablation rates (Fausto et al., 2016, 2021; Mattingly et al., 2018; Neff, 2018). The frequency of ARs impinging on Greenland is increasing (Mattingly et al., 2016), driven by more common highly-amplified jet-stream patterns (Francis and Skific, 2015).

The moisture and heat transport by the AR was further examined by tracking air mass backward for 4 d from the ice sheet Summit. The backward trajectories agreed with the distribution of the southerly flow, confirming a strong WMA transport from the abnormally warm North Atlantic across the Labrador Sea to the summit of the ice sheet (Figure S3 and Figure 2f). The WMA transport included convergence, ensuring an intensification of heat and moisture delivery.

From 10 August to 13 August, the air mass flowed with internal heat conservation (Figure S4b). From hours −14 to zero (00–14 UTC on 14 August), as the air mass was uplifted over the ice sheet (Figure S4a), the air mass cooled 16 K by expansion, and that cooling was partially offset by ~8 K heating from condensation (Figure S4b). Concurrently,

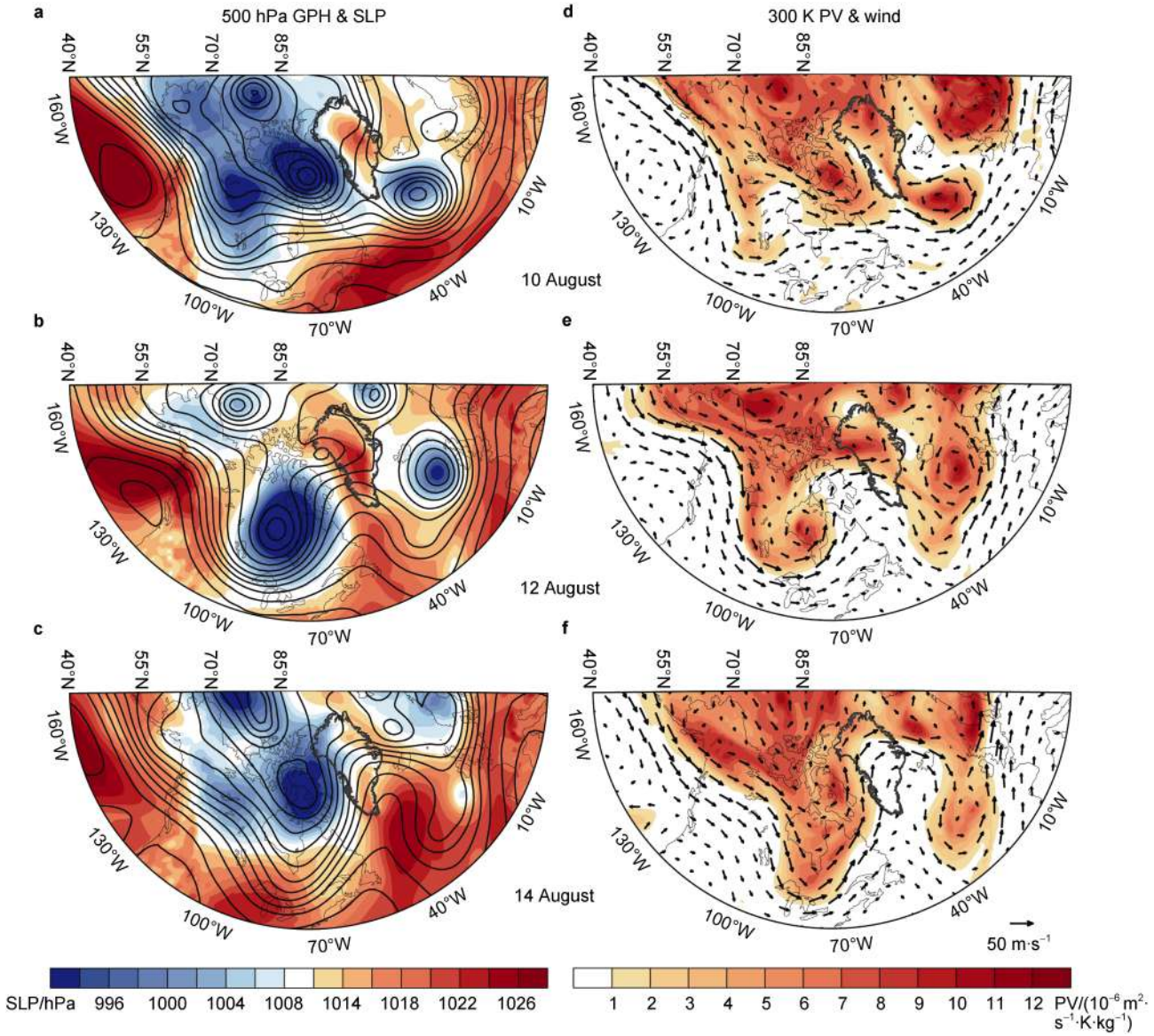

Figure 2 Dynamic mechanism of the formation and maintenance of cyclone over Baffin Island. Daily mean 500-hPa geopotential height (GPH, contour, units: m) and sea level pressure (SLP, shaded) on 10 August (**a**), 12 August (**b**) and 14 August (**c**), 2021. The contours are drawn for every 50 m. (**d**)–(**f**) as per (**a**)–(**c**), but for the 330 K potential vorticity (PV, shaded) and horizontal wind (arrows), illustrating the formation and evolution of a trough or ridge.

the air parcel humidity was reduced by water droplet formation (Figure S4c). The diabatic heating maintained the air parcel temperature around the melting point, which favored rain rather than snow as high as Summit Station.

3.3 Rain produced by low-level liquid clouds

Except for the latent and sensible heating effects of the WMA, cloud microphysical process could also play a key role in the formation of liquid precipitation instead of snowfall. Evident from the cloud images retrieved by ESA MetOp satellites, clouds had developed over Greenland on 13 August, most of which included supercooled water droplets (Figure S5a). On 14 August, the liquid water path (LWP) increased along the AR (Figure S5b and Figure 3b), indicating that the intrusion of WMA formed new liquid cloud droplets through condensation.

ESA MetOp-A satellite observations show that the cloud top temperatures ranged 261–273 K (264 K on average) (Figure 3c), which were higher than the value (around 258 K) for the Bergeron–Findeisen–Wegener (BFW) process to likely occur (Korolev and Isaac, 2003). That said, even if the condensation nuclei were introduced into the cloud, the BFW process is ineffective for it is a mechanism of snowfall formation through sublimation growth of ice crystals (Wegener, 1911; Bergeron, 1935, 1949). On the other hand, if the BFW process was active, the snowfall "that" it produced could not melt in such a short distance under the established temperature vertical profile

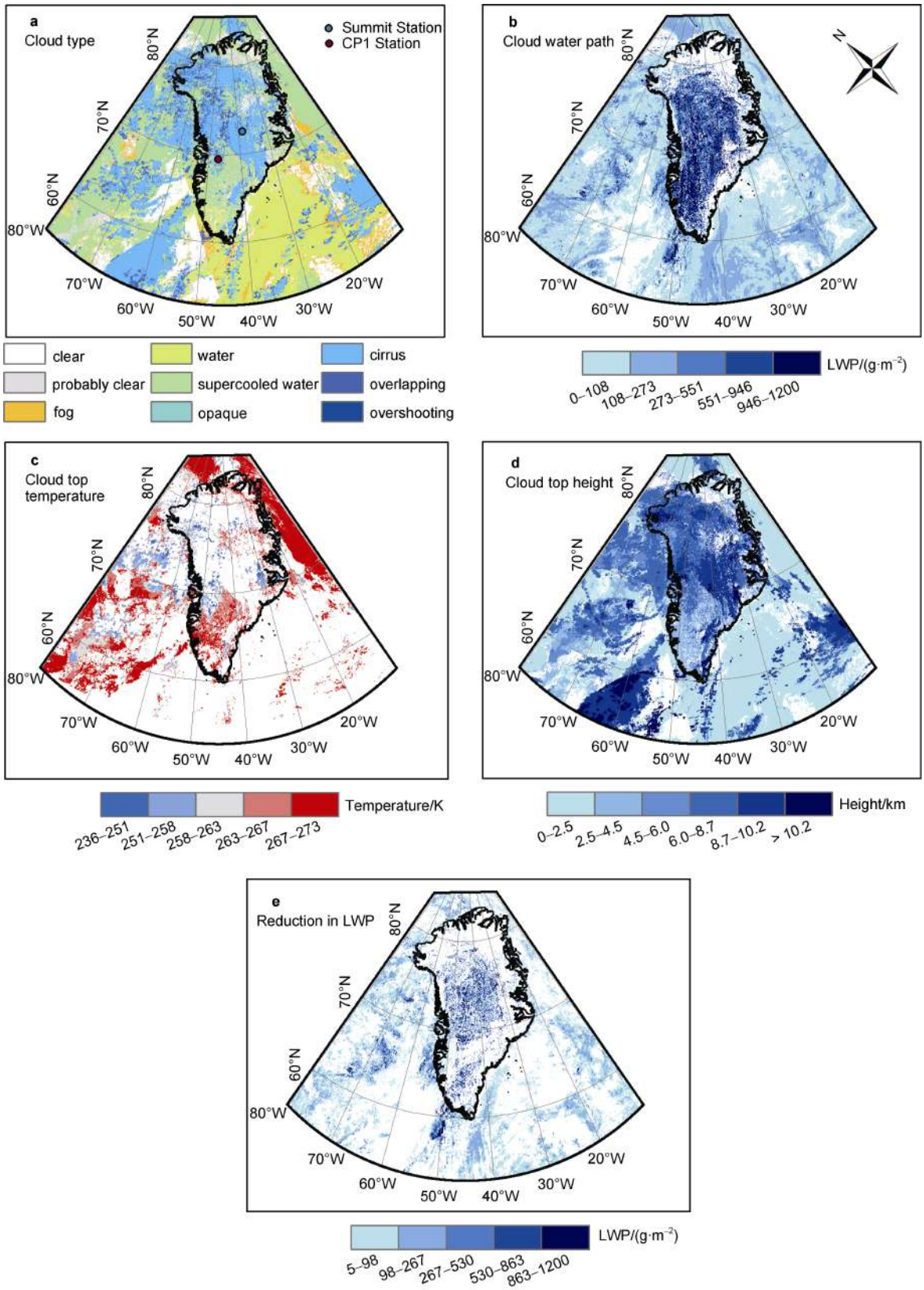

Figure 3 Cloud physical characteristics over Greenland from the ESA MetOp-A satellite retrievals during the rainfall event on 14 August, 2021. **a**, The types of clouds; **b**, The LWP during the rainfall event; **c**, The cloud top temperature; **d**, The top height of various cloud types; **e**, The reduction of LWP during the rainfall event.

(Figure 1c), since the liquid-phase clouds were too low (<2 km above the ground) during the rainfall event (Figure 3d).

Previous studies on the formation mechanism of warm cloud rainfall in middle and low latitudes found that the wet air flow could aggravate the cloud turbulence and promote the growth of cloud particles, generating larger cloud droplets (Pruppacher and Klett, 1997; Devenish et al., 2012; Wyszogrodzki et al., 2013). The turbulent process amplified the size differentiation of droplets in the liquid clouds, leading to the further coalescence growth of droplets due to differing droplet falling speeds (Ayala et al., 2008; Woittiez et al., 2009). Once the weights of the droplets exceed the carrying capacity of the updraft, falling rain droplets occur (Rosenfeld et al., 2013). In the supercooled water cloud region, due to the existence of a large number of liquid-phase cloud droplets, the collision and growth of cloud droplets could be intensified with the continuous invasion of WMA, producing liquid precipitation without the BFW process.

Direct measurement of the microphysical processes of cloud droplet evolution were not accessible in this case. We thus estimated the rainfall produced by the water vapor convergence on 14 August based on ERA5 (see "Data and methods" section), and compared with the AWS rainfall observations at CP1 on the same day, which is located in the accumulation area of the ice sheet southwest of the Summit Station at 2022 m above sea level (Figure 3a). Results show that the newly formed liquid clouds due to water vapor convergence contributed most (~11 mm of 14 mm) of the rainfall amount, while the contribution of the direct reduction of the original liquid cloud was about 658 $g \cdot m^{-2}$ (Figure 3e), which was equivalent to about only ~1 mm rainfall. These two parts contributed a total of ~11 mm rainfall, lower than the observed total (14 mm). For the Summit Station, the decrease in the original liquid cloud and the water vapor convergence contributed ~1 mm and 6 mm to the rainfall amount, respectively.

4 Discussions and conclusions

The intrusion of strong WMA was a main cause of the widespread rainfall over the Greenland Ice Sheet on 14 August, 2021, which was initiated and maintained by a cyclonic system stalling to the west over Baffin Island. The formation mechanism of this cyclone was associated with a deep closed low pressure system isolated from the polar vortex over Hudson Bay. Due to southward and downward advections of high potential vorticity associated with the dominant subtropical high over the Northeastern Pacific, the deep cyclone intensified over the Hudson Bay and then displaced northward to Baffin Island (Figure 4). This cyclone with the downstream anticyclonic circulation rendered pronounced southerly flow prevailing from the Labrador Sea to Greenland in the troposphere, which brought in warm and moisture air to the inland areas over Greenland.

For the thermal process, most of the air mass was originated from the mid- to low-troposphere and advected in the low level near the ocean surface and maintained the conservation of heat content until it reached Greenland. As such, the southwesterly flow could deliver to Greenland the heat absorbed over the Labrador Sea and the North American Atlantic sector, where the sea surface temperature was 1 to 2 °C above normal according to ERA5 reanalysis (Figure S6). As a consequence of the WMA advection and uplift with cooling partially offset by condensational heating, the temperature from ground to 250 hPa over the summit area was ~2 °C higher than the previous record value since at least 1995. The higher temperature favored rainfall at the expense of snowfall.

This study suggested that the low-level liquid clouds over ice sheet played an important role in generating rainfall. As the WMA invaded northward and inland over the ice sheet, it produced liquid droplets through condensation and promoted a rain droplet collection increase by increasing the cloud turbulence, eventually generating rain drops through gravitational collision. This study proposed a reasonable inference based on the observations of cloud phase and temperature. The full microphysical evolutions of the collision and coalescence have however yet to be documented.

Further analysis indicates that the clouds in ERA5 generated over the southwestern edge of the ice sheet from the afternoon of 13 August, and gradually developed and extended to the inland areas, reaching the maximum extent at 5 to 7 UTC on the 14 August (see Movie S in "Supplementary Figures and Movie" online). However, compared with satellite observations (Figure 3b), ERA5 could hardly reproduce the large extension of liquid clouds over the inland area of the ice sheet, possibly leading to an underestimation of the rainfall extent in this area (Figure 1a).

The sixth report of IPCC Working Group I suggests that the ocean south of Greenland is an area of frequent marine heat waves (MHW) (Frölicher et al., 2018; Fox-Kemper, 2021). In this study, we contend that MHWs and a breaking polar vortex are critical preconditions for suitable atmospheric circulation configurations of WMA, of which intruding into the inland areas of the ice sheet and accompanying rainfall events will no longer be so rare. In this regard, rainfall events are an additional factor contributing to increasing ice sheet melting in a warming Arctic.

Author contributions Xiao C D, Dou T F and Box J E designed the study. Dou T F, Xie Z W, Yang Q, Yang Y F, Teng S W and Xu G J analysed the data and produced the figures. Dou T F, Xie Z W, Xiao C D and Box J E wrote the manuscript with contributions from all authors.

Conflict of interest The authors declare no competing interests.

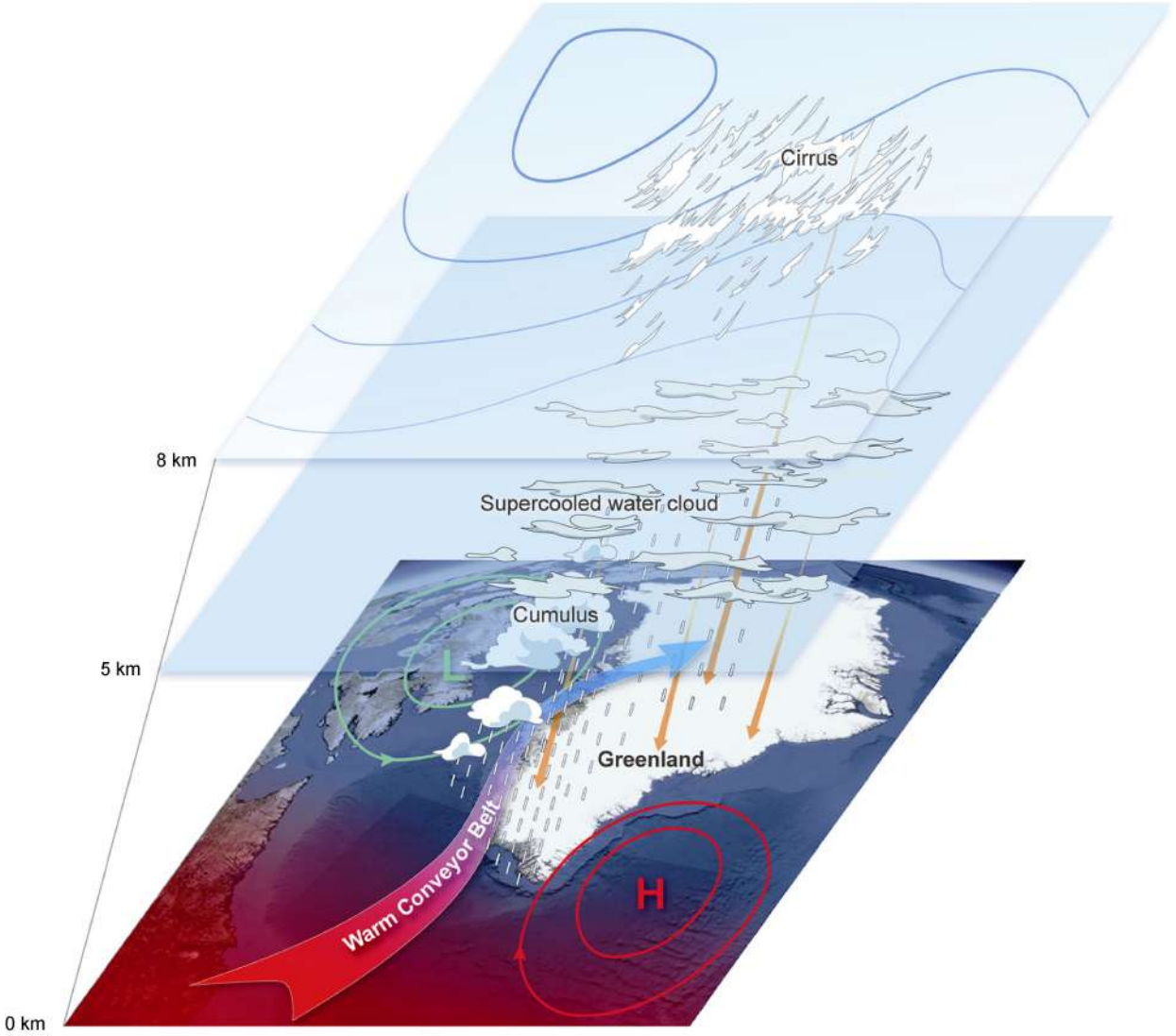

Figure 4 Conceptional illustration of the major formation mechanism of the rainfall event over the Greenland Ice Sheet on 14 August, 2021.

Data availability statement The data of air temperature, precipitation and surface albedo observed by AWS used here can be accessed through https://www.envidat.ch/data-api/gcnet/. The data that support the analysis of cloud physics are available at https://www.ncei.noaa.gov/data/avhrr-hirs-reflectance-and-cloud-properties-patmosx/access/. The ERA5 reanalysis data is available from https://cds.climate.copernicus.eu/cdsapp#!/search?type=dataset.

Acknowledgments This study is supported by the National Key Research & Development Program of China (Grant no. 2018YFC1406104). The precipitation measurements at CP1 were conducted by Geological Survey of Denmark and Greenland (GEUS) under support from the Danish Ministry of Climate, Energy and Utilities via The Programme for Monitoring of the Greenland Ice Sheet (PROMICE), the INTAROS project under the European Union's Horizon 2020 Research and Innovation Program under grant agreement no. 727890 and the Greenland Integrated Observing System (GIOS) of Denmark. We appreciate two anonymous reviewers, and Guest Editor Dr. Tong Zhang for their constructive comments that have further improved the manuscript.

References

Ayala O, Rosa B, Wang L P. 2008. Effects of turbulence on the geometric collision rate of sedimenting droplets. Part 2. Theory and parameterization. New J Phys, 10(7): 075016, doi:10.1088/1367-2630/10/7/075016.

Bergeron T. 1935. On the physics of cloud and precipitation. Lisbon: UGGI, 2: 156.

Bergeron T. 1949. The problem of artificial control of rainfall on the globe: II. the coastal orographic maxima of precipitation in autumn and winter. Tellus, 1(3): 15-32, doi:10.1111/j.2153-3490.1949.tb01264.x.

Box J E, Wehrlé A, van As D, et al. 2022. Greenland ice sheet rainfall, heat and albedo feedback impacts from the mid-August 2021 atmospheric river. Geophys Res Lett, 49(11): e2021GL097356, doi:10.1029/2021gl097356.

Devenish B J, Bartello P, Brenguier J L, et al. 2012. Droplet growth in warm turbulent clouds. QJR Meteorol Soc, 138(667): 1401-1429, doi:10.1002/qj.1897.

Dou T F, Xiao C D, Liu J P, et al. 2019. A key factor initiating surface ablation of Arctic sea ice: earlier and increasing liquid precipitation.

Cryosphere, 13(4): 1233-1246, doi:10.5194/tc-13-1233-2019.

Dou T F, Xiao C D, Liu J P, et al. 2021. Trends and spatial variation in rain-on-snow events over the Arctic Ocean during the early melt season. Cryosphere, 15(2): 883-895, doi:10.5194/tc-15-883-2021.

Dou T F, Pan S F, Bintanja R, et al. 2022. More frequent, intense, and extensive rainfall events in a strongly warming Arctic. Earth Future, 10(10): e2021EF002378, doi:10.1029/2021ef002378.

Doyle S H, Hubbard A, van de Wal R S W, et al. 2015. Amplified melt and flow of the Greenland ice sheet driven by late-summer cyclonic rainfall. Nature Geosci, 8(8): 647-653, doi:10.1038/ngeo2482.

Eckhardt S, Stohl A, Wernli H, et al. 2004. A 15-year climatology of warm conveyor belts. J Climate, 17(1): 218-237, doi:10.1175/1520-0442(2004)017<0218: aycowc>2.0.co;2.

Fausto R S, van As D, Box J E, et al. 2016. The implication of nonradiative energy fluxes dominating Greenland ice sheet exceptional ablation area surface melt in 2012. Geophys Res Lett, 43(6): 2649-2658, doi:10.1002/2016gl067720.

Fausto R S, van As D, Mankoff K D, et al. 2021. Programme for Monitoring of the Greenland Ice Sheet (PROMICE) automatic weather station data. Earth Syst Sci Data, 13(8): 3819-3845, doi:10.5194/essd-13-3819-2021.

Fettweis X, Franco B, Tedesco M, et al. 2013. Estimating the Greenland ice sheet surface mass balance contribution to future sea level rise using the regional atmospheric climate model MAR. Cryosphere, 7(2): 469-489, doi:10.5194/tc-7-469-2013.

Fox-Kemper B. 2021. Ocean, cryosphere and sea level change. New Orleans, Louisiana, USA: AGU Fall Meeting 2021.

Francis J, Skific N. 2015. Evidence linking rapid Arctic warming to mid-latitude weather patterns. Phil Trans R Soc A, 373(2045): 20140170, doi:10.1098/rsta.2014.0170.

Frölicher T L, Fischer E M, Gruber N. 2018. Marine heatwaves under global warming. Nature, 560(7718): 360-364, doi:10.1038/s41586-018-0383-9.

Han W, Xiao C, Dou T, et al. 2018. Arctic has been going through a transition from solid precipitation to liquid precipitation in spring. Chin Sci Bull, 63: 1154-1162, doi:10.1360/N972018-00088 (in Chinese with English abstract).

Hersbach H, Bell B, Berrisford P, et al. 2020. The ERA5 global reanalysis. QJR Meteorol Soc, 146(730): 1999-2049, doi:10.1002/qj.3803.

Key J, Liu Y, Wang X. 2015. Program: NOAA Climate Data Record (CDR) of AVHRR Polar Pathfinder (APP) Cryosphere, Version 1.0. NOAA National Centers for Environmental Information (NCEI).

Korolev A, Isaac G. 2003. Phase transformation of mixed-phase clouds. QJR Meteorol Soc, 129(587): 19-38, doi:10.1256/qj.01.203.

Mattingly K S, Ramseyer C A, Rosen J J, et al. 2016. Increasing water vapor transport to the Greenland Ice Sheet revealed using self-organizing maps. Geophys Res Lett, 43(17): 9250-9258, doi:10.1002/2016gl070424.

Mattingly K S, Mote T L, Fettweis X. 2018. Atmospheric river impacts on Greenland ice sheet surface mass balance. J Geophys Res Atmos, 123(16): 8538-8560, doi:10.1029/2018jd028714.

McCrystall M R, Stroeve J, Serreze M, et al. 2021. New climate models reveal faster and larger increases in Arctic precipitation than previously projected. Nat Commun, 12: 6765, doi:10.1038/s41467-021-27031-y.

Neff W. 2018. Atmospheric rivers melt Greenland. Nat Clim Change, 8(10): 857-858, doi:10.1038/s41558-018-0297-4.

Neff W, Compo G P, Martin Ralph F, et al. 2014. Continental heat anomalies and the extreme melting of the Greenland ice surface in 2012 and 1889. J Geophys Res Atmos, 119(11): 6520-6536, doi:10.1002/2014jd021470.

Newell R E, Newell N E, Zhu Y, et al. 1992. Tropospheric Rivers? – A pilot study. Geophys Res Lett, 19(24): 2401-2404, doi:10.1029/92g l02916.

Niwano M, Box J E, Wehrlé A, et al. 2021. Rainfall on the Greenland ice sheet: present-day climatology from a high-resolution non-hydrostatic polar regional climate model. Geophys Res Lett, 48(15): e2021GL092942, doi:10.1029/2021gl092942.

Pavolonis M J, Heidinger A K, Uttal T. 2005. Daytime global cloud typing from AVHRR and VIIRS: algorithm description, validation, and comparisons. J Appl Meteorol, 44(6): 804-826, doi:10.1175/jam2236.1.

Pinzon J, Tucker C. 2014. A non-stationary 1981-2012 AVHRR $NDVI_{3g}$ time series. Remote Sens, 6(8): 6929-6960, doi:10.3390/rs6086929.

Pruppacher H, Klett J. 1997. Microphysics of clouds and precipitation, 2nd Edition. Dordrecht: Kluwer Academic, 954.

Ralph F M, Neiman P J, Wick G A. 2004. Satellite and CALJET aircraft observations of atmospheric rivers over the eastern north Pacific Ocean during the winter of 1997/98. Mon Wea Rev, 132(7): 1721-1745, doi:10.1175/1520-0493(2004)132<1721:sacaoo>2.0.co;2.

Ramirez R. 2021. Rain fell at the normally snowy summit of Greenland for the first time on record. CNN News. (2021-08-19) [2022-08-20]. https://edition.cnn.com/2021/08/19/weather/greenland-summit-rain-climate-change/index.html.

Reijmer C H, van den Broeke M R, Fettweis X, et al. 2012. Refreezing on the Greenland ice sheet: a comparison of parameterizations. Cryosphere, 6(4): 743-762, doi:10.5194/tc-6-743-2012.

Rennermalm A K, Smith L C, Chu V W, et al. 2013. Evidence of meltwater retention within the Greenland ice sheet. Cryosphere, 7(5): 1433-1445, doi:10.5194/tc-7-1433-2013.

Rosenfeld D, Chemke R, DeMott P, et al. 2013. The common occurrence of highly supercooled drizzle and rain near the coastal regions of the western United States. J Geophys Res Atmos, 118(17): 9819-9833, doi:10.1002/jgrd.50529.

Scambos T, Stroeve J, Koenig L, et al. 2021. Rain at the summit of Greenland. National Snow and Ice Data Center, http://nsidc.org/greenland-today/2021/08/rain-at-the-summit-of-greenland/.

Sprenger M, Wernli H. 2015. The LAGRANTO Lagrangian analysis tool – version 2.0. Geosci Model Dev, 8: 2569-2586, doi:10.5194/gmd-8-2569-2015, 2015.

Steffen K, Box J, Abdalati W. 1996. Greenland climate network: GC-Net. US Army Cold Regions Reattach and Engineering (CRREL), CRREL Special Report, 98-103.

Vandecrux B, Fausto R S, van As D, et al. 2020. Firn cold content evolution at nine sites on the Greenland ice sheet between 1998 and 2017. J Glaciol, 66(258): 591-602, doi:10.1017/jog.2020.30.

van den Broeke M, van As D, Reijmer C, et al. 2004. Assessing and improving the quality of unattended radiation observations in Antarctica. J Atmos Oceanic Technol, 21(9): 1417-1431, doi:10.1175/1520-0426(2004)021<1417: aaitqo>2.0.co;2.

Wegener A. 1911. Thermodynamik der Atmosphäre. Leipzig: J. A. Barth.

Woittiez E J P, Jonker H J J, Portela L M. 2009. On the combined effects of turbulence and gravity on droplet collisions in clouds: a numerical study. J Atmos Sci, 66(7): 1926-1943, doi:10.1175/2005jas2669.1.

Wyszogrodzki A A, Grabowski W W, Wang L P, et al. 2013. Turbulent collision-coalescence in maritime shallow convection. Atmos Chem Phys, 13(16): 8471-8487, doi:10.5194/acp-13-8471-2013.

Yang D Q, Ishida S, Goodison B, et al. 1999. Bias correction of daily precipitation measurements for Greenland. J Geophys Res, 104: 6171-6181, doi:10.1029/1998JD200110.

Supplementary Figures and Movie

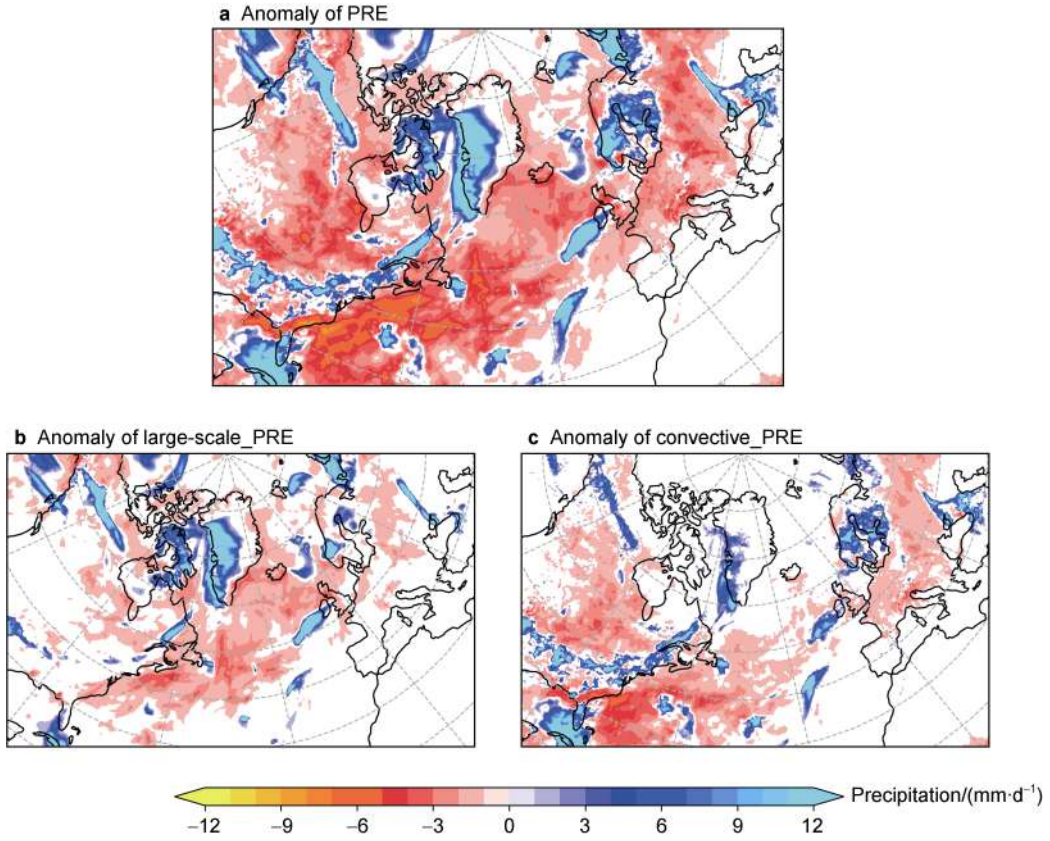

Figure S1 Anomalies of ERA5 daily mean total precipitation (**a**), large-scale precipitation (**b**) and convective precipitation (**c**), on 14 August 2021, relative to the same period of 1979–2020 mean. Only the absolute values of precipitation anomalies greater than 1 mm·d^{-1} are shaded.

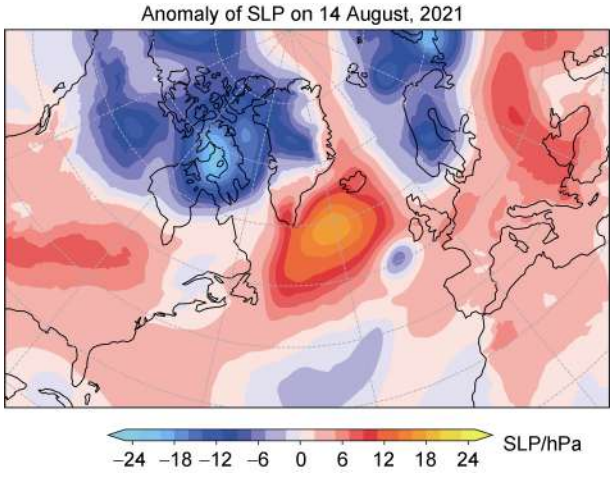

Figure S2 Anomaly of ERA5 daily mean air pressure at mean sea level (SLP) on 14 August 2021, relative to the same period of 1979–2020 mean.

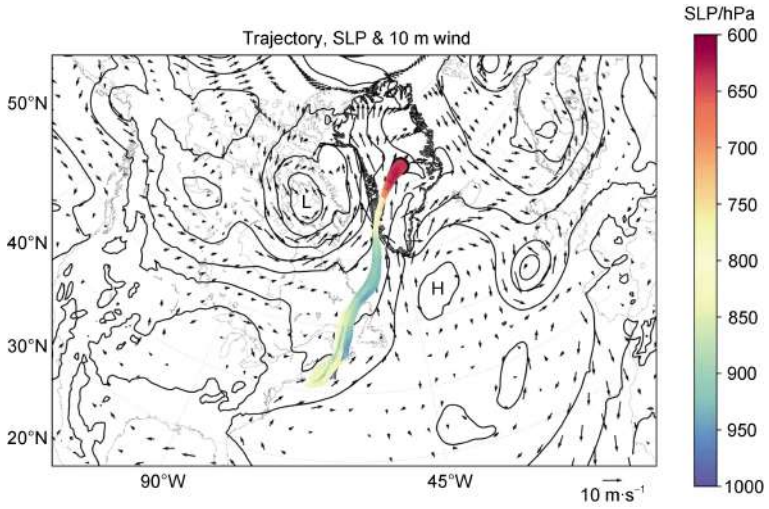

Figure S3 Daily mean ERA5 sea level pressure (SLP) and 10 m horizontal wind (arrows) above the ground on 14 August, 2021. The color shaded curves are the trajectories tracked backward for 4 d started at 14:00 UTC on 14 August 2021. The starting points are equidistantly distributed every 10 km in a circle of radius 50 km around the Summit Station of Greenland. Contours are drawn for every 5 hPa. "L" and "H" signify the low and high pressure, respectively. Color shading represents air pressure.

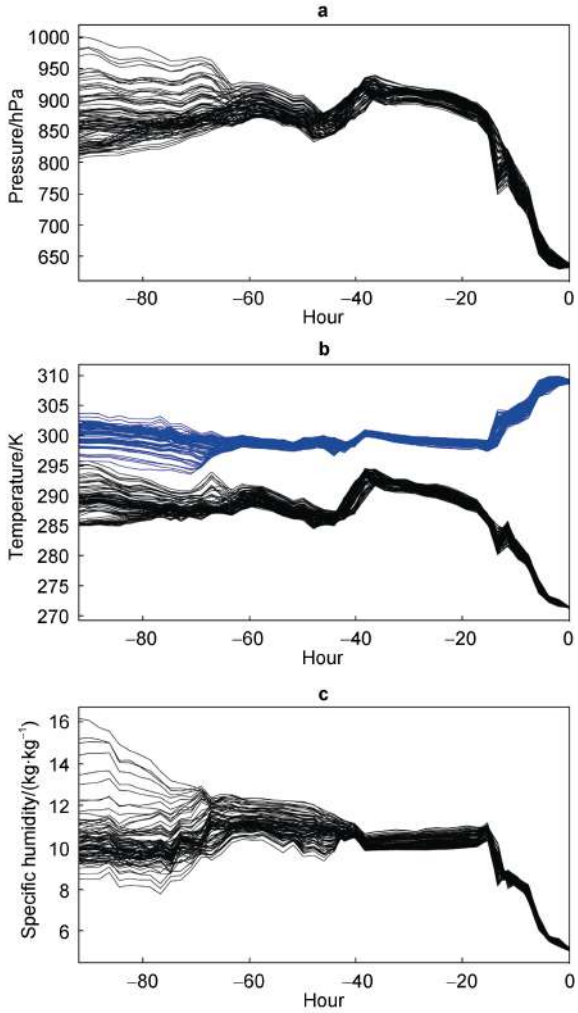

Figure S4 Time series of pressure (**a**), temperature (black) and potential temperature (blue) (**b**) and specific humidity (**c**) along the 4-day backward trajectories from the Summit Station (see "Methods").

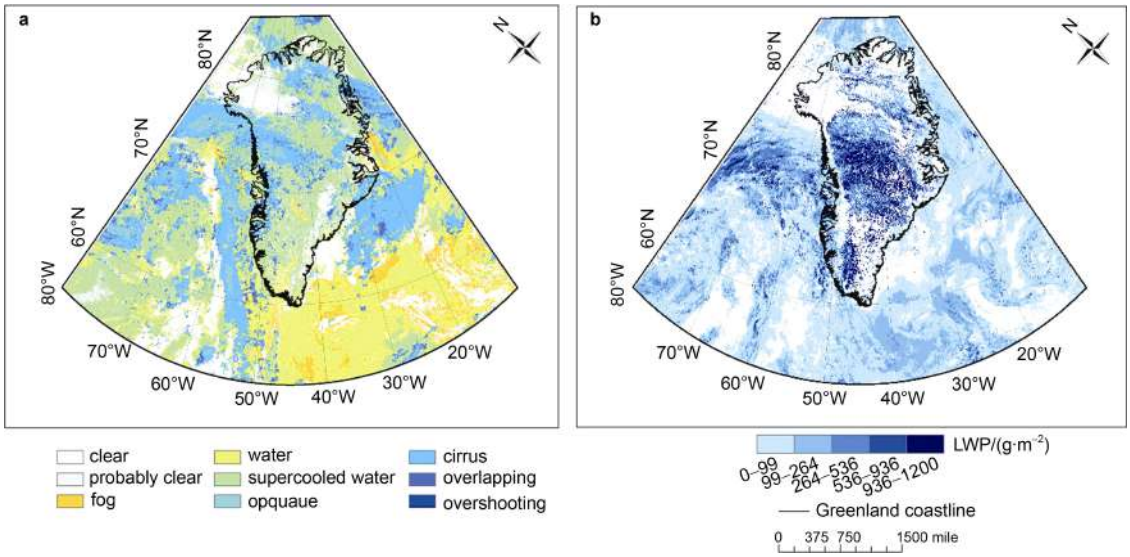

Figure S5 The types of clouds over Greenland from the ESA MetOP and NOAA-16 satellites observations during the rainfall event on August 13 (**a**); The LWP during the rainfall event (**b**).

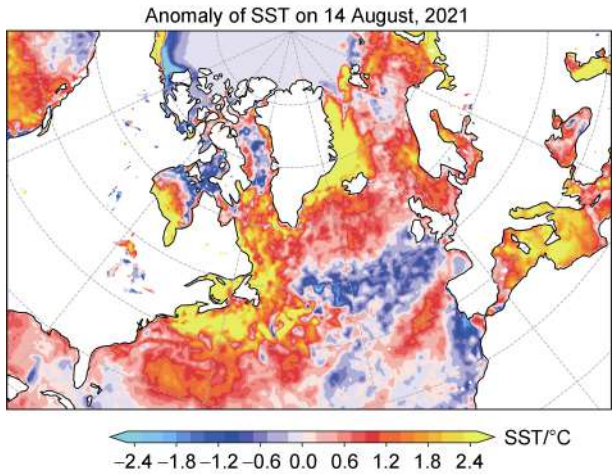

Figure S6 Anomaly of ERA5 daily mean sea surface temperature (SST) on 14 August 2021, relative to the same period of 1979–2020 mean.

Movie S Suppercooled cloud dynamic over Greenland based on ERA5.

The movie is available online at https://aps.chinare.org.cn/EN/10.12429/j.advps.2022.0016.